HHS Public Access

Author manuscript

*Science*. Author manuscript; available in PMC 2018 February 27.

Published in final edited form as:

*Science*. 2018 January 05; 359(6371): 97–103. doi:10.1126/science.aan4236.

# Gut microbiome modulates response to anti–PD-1 immunotherapy in melanoma patients

*A full list of authors and affiliations appears at the end of the article.*

Pre-clinical mouse models suggest that the gut microbiome modulates tumor response to checkpoint blockade immunotherapy; however, this has not been well-characterized in human cancer patients. Here we examined the oral and gut microbiome of melanoma patients undergoing anti-PD-1 immunotherapy (n=112). Significant differences were observed in the diversity and composition of the patient gut microbiome of responders (R) versus non-responders (NR). Analysis of patient fecal microbiome samples (n=43, 30R, 13NR) showed significantly higher alpha diversity ($p<0.01$) and relative abundance of Ruminococcaceae bacteria ($p<0.01$) in responding patients. Metagenomic studies revealed functional differences in gut bacteria in R including enrichment of anabolic pathways. Immune profiling suggested enhanced systemic and anti-tumor immunity in responding patients with a favorable gut microbiome, as well as in germ-free mice receiving fecal transplants from responding patients. Together, these data have important implications for the treatment of melanoma patients with immune checkpoint inhibitors.

Tremendous advances have been made in the treatment of melanoma and other cancers using immune checkpoint inhibitors targeting the cytotoxic T-lymphocyte-associated antigen (CTLA-4) and the programmed death 1 (PD-1) protein, however responses to these therapies are often heterogeneous and not durable (1–3). It has recently emerged that factors beyond tumor genomics influence cancer development and therapeutic responses (4–7), including host factors such as the gastrointestinal (gut) microbiome (8–10). A number of studies have shown that the gut microbiome may influence anti-tumor immune responses via innate and adaptive immunity (11, 12), and that therapeutic responses may be improved via its modulation (13, 14), however this has not been extensively studied in cancer patients.

To better understand the role of the microbiome in response to immune checkpoint blockade, we prospectively collected microbiome samples from patients with metastatic melanoma starting treatment with anti-PD-1 therapy (n=112 patients) (fig. S1 and table S1). Oral (buccal) and gut (fecal) microbiome samples were collected at treatment initiation, and

**Corresponding author. jwargo@mdanderson.org.
*These authors contributed equally to this work.
†Present address: University of Rochester James P. Wilmot Cancer Center, Rochester, NY 14642, USA.
‡Present address: A.C.Camargo Cancer Center, São Paolo, Brazil.
§Present address: Moffitt Cancer Center, Tampa, FL 33612, USA.
‖Present address: Harvard University, Cambridge, MA 02138, USA.
¶Present address: MedImmune, Gaithersburg, MD 20878, USA.
#These authors contributed equally to this work.

The other authors declare no competing interests.

Supplementary Materials
www.sciencemag.org/cgi/content/full/science.aan4236/DC1

tumor biopsies and blood samples were collected at matched pre-treatment time points when possible to assess for genomic alterations, as well as the density and phenotype of tumor-infiltrating and circulating immune cell subsets (Fig. 1A and fig. S2). Taxonomic profiling via 16S rRNA gene sequencing was performed on all available oral and gut samples, with metagenomic whole genome shotgun (WGS) sequencing on a subset (n=25). Eligible patients (n=89) were classified as responders (R; n=54) versus non-responders (NR; n=35) based on radiographic assessment using the Response Evaluation Criteria in Solid Tumors (RECIST 1.1) criteria (15) at 6 months after treatment initiation. Patients were classified as R if they achieved an objective response (complete or partial response or stable disease lasting at least 6 months), versus NR if they progressed on therapy or had stable disease lasting less than 6 months. This classification accounts for the subset of patients who may derive long-term disease benefit despite not achieving a bona fide RECIST response, and has been employed in numerous published studies of patients on checkpoint blockade (16–19). Of note, patients in R versus NR groups were similar with respect to age, gender, primary type, prior therapy, concurrent systemic therapy and serum lactate dehydrogenase (LDH) (table S2). Prior genomic analyses have demonstrated that patients with tumors having a higher mutational load are more likely to respond to anti-CTLA-4 (16, 20, 21) or anti-PD-1 therapy (21–24), however a high mutational load alone appears neither sufficient nor essential for response. In this cohort, the total number and specific melanoma driver mutations were within comparable parameters between R and NR following anti-PD-1 therapy (fig. S3), though the number of tumors available for sequencing (n=10, R=7, NR=3) was limited and may have reduced our ability to detect a significant association between mutational burden and response.

We first assessed the landscape of the oral and gut microbiome in all available samples in patients (n=112) with metastatic melanoma via 16S sequencing, noting that both communities were relatively diverse, with a high abundance of Lactobacillales in the oral microbiome and Bacteroidales in the fecal microbiome (Fig. 1B). Bipartite network analysis (25) demonstrated a clear separation of community structure between the oral and fecal microbiomes in terms of both matched and aggregate samples (fig. S4), suggesting that these communities are distinct. Loss of microbial diversity (dysbiosis) is associated with chronic health conditions (26–28) and cancer (8–10), and is also associated with poor outcomes to certain forms of cancer therapy including allogeneic stem cell transplant (29). Based on these data, we examined the diversity of the oral and gut microbiomes in eligible patients on anti-PD1 therapy, and found that alpha diversity of the gut microbiome was significantly higher in R (n=30) compared to NR (n=13) using several indices ($p<0.01$, Fig. 1C and fig. S5). No significant differences were observed in the oral microbiome (R=54, NR=32, $p=0.11$, fig. S6). We then tested the relationship of diversity and progression-free survival (PFS) in our cohort by stratifying patients based on tertiles of Inverse Simpson scores, demonstrating that patients with a high diversity in the fecal microbiome had significantly prolonged PFS compared to those with intermediate or low diversity ($p=0.02$ and 0.04, respectively; Fig. 1, D and E, and fig. S7). No differences in PFS were noted when comparing diversity of the oral microbiome (fig. S8). Importantly, upon visualizing beta diversity weighted UniFrac distances (30) by principal coordinate analysis, we found a

notable clustering effect by response status in the gut microbiome of these patients, which was not observed in the oral microbiome (Fig. 1F and fig. S8E).

Since compositional differences in the microbiome may also influence cancer development and response to therapy (12, 14, 15, 23), we sought to determine if differences existed in the oral or gut microbiomes of R and NR to anti-PD-1 therapy. To test this, we first compared an enrichment of operational taxonomic units (OTUs) in R versus NR, demonstrating that distinct sets of rare low abundance OTUs were associated with response to anti-PD-1 therapy, with enrichment of Clostridiales in R and Bacteroidales in NR in the gut microbiome ($p<0.01$, Fig. 2, A and B, and fig. S9, A and C). No significant differences in enrichment were noted in the oral microbiome of R versus NR (fig. S9, B and D, and fig. S10). To further explore these findings, we performed high dimensional class comparisons via linear discriminant analysis of effect size (LEfSe) (31), which again demonstrated differentially abundant bacteria in the fecal microbiome of R versus NR to anti-PD-1 therapy, with Clostridiales/Ruminococcaceae enriched in R and Bacteroidales enriched in NR (Fig. 2, C and D). No major differences were observed in the oral microbiome between R and NR, with the exception of higher Bacteroidales in NR to anti-PD-1 therapy (fig. S11). Pairwise comparisons were then performed for bacterial taxa at all levels by response. In addition to confirming the previous taxonomic differences, these analyses identified the *Faecalibacterium* genus as significantly enriched in R (Fig. 2E and table S3). Metagenomic WGS further confirmed enrichment of *Faecalibacterium* species in addition to others in R, while *Bacteroides thetaiotaomicron, Escherichia coli*, and *Anaerotruncus colihominis* were enriched in NR (Fig. 2F and table S4). Importantly, the gut microbiome was shown to be relatively stable over time in a limited number of longitudinal samples tested (fig. S12).

We next asked whether bacterial composition and abundances within the gut and/or oral microbiomes of patients were associated with a specific treatment outcome to anti-PD-1 therapy. We grouped all identified OTUs into clusters of related OTUs (crOTUs) via construction of a phylogenetic tree from sequence alignment data (32). This technique involves comparison of abundances of different potential groupings of bacteria based on 16S sequence similarity and helps address the sparse distribution of OTU abundances observed in the absence of this approach (fig. S13). Unsupervised hierarchical clustering of crOTU abundances within the gut and oral microbiomes was then performed without input of response data. We found that patients segregated into 2 distinct community types. Type 1 comprised entirely of R and was enriched for Clostridiales, whereas Type 2 comprised a mixture of R and NR ($p=0.02$) and was enriched for Bacteroidales (Fig. 3A). To better understand compositional differences between these crOTU community types, we again performed pairwise comparisons of the gut microbiota, and identified a pattern very similar to that seen when clustering by response, with Clostridiales/Ruminococcaceae enriched in Type 1, and Bacteroidales enriched in Type 2 (fig. S14A and table S5). Further, these communities clustered distinctly using principal coordinate analysis of weighted Unifrac distances (fig. S14B). Analysis of crOTUs in the oral microbiome revealed no apparent relationship to treatment response (fig. S15, A and B).

To explore how specific bacterial taxa impact patient treatment response, we compared PFS following anti-PD-1 therapy as it related to the “top hits” consistently observed across our

analyses. From the Ruminococcaceae family of the Clostridiales order, we focused on the *Faecalibacterium* genus in R, and Bacteroidales order in NR, and stratified patients into high versus low categories based on the median relative abundance of these taxa in the gut microbiome. Patients with high *Faecalibacterium* abundance had a significantly prolonged PFS versus those with a low abundance (p=0.03). Conversely, patients with a high abundance of Bacteroidales had a shortened PFS compared to those with a low abundance (p=0.05, Fig. 3D). This is in line with recently published data in a small cohort of patients on CTLA-4 blockade, where patients with a higher abundance of *Faecalibacterium* had a prolonged PFS compared to those with a higher abundance of Bacteroidales in the gut microbiome (33). In addition, univariate Cox proportional hazards analyses demonstrated that the strongest microbial predictors of response to anti-PD-1 therapy were alpha diversity [Intermediate hazard ratio (HR)=3.60, 95% C.I.=1.02-12.74; Low HR=3.57, 95% confidence interval (C.I.)=1.02-12.52], and abundance of *Faecalibacterium* (HR=2.92, 95% C.I.=1.08-7.89) and Bacteroidales (HR= 0.39, 95% CI=0.15-1.03) in the fecal microbiome. There was no association found between PFS and stage in our cohort. Our final multivariate model was selected by forward stepwise selection and included *Faecalibacterium* abundance (HR=2.95, 95% C.I.=1.31-7.29, p=0.03) and prior immunotherapy (HR=2.87, 95% C.I.=1.10-7.89, p=0.03) (table S6). Abundance of *Faecalibacterium* and Bacteroidales also outperformed relevant clinical variables in receiver operating characteristic curve (ROC) analysis (fig. S16).

Next, we sought to gain insight into the mechanism through which the gut microbiome may influence response to anti-PD-1 therapy, and first conducted functional genomic profiling of gut microbiome samples via metagenomic WGS sequencing (n=25) in R (n=14) vs NR (n=11). Organism-specific gene hits were assigned to the Kyoto Encyclopedia of Genes and Genomes (KEGG) orthology (KO), and based on these annotations, metagenomes for each sample were reconstructed into metabolic pathways using the MetaCyc hierarchy of pathway classifications (34, 35). Unsupervised hierarchical clustering of predicted pathway enrichment identified two groups of patient samples, with response rates of 69.2% and 41.7% (Fig. 3E). A similar pattern was also noted for KO-abundances with 70.6% and 37.5% response rates (fig. S17). Comparisons of pathway enrichment across these groups showed changes in metabolic functions, with anabolic functions predominating in R including amino acid biosynthesis (Fig. 3E), which may promote host immunity (36), whereas catabolic functions predominated in NR (Fig. 3E, fig. S16, and table S7).

There is clear evidence in pre-clinical models that differential composition of the gut microbiome may influence therapeutic responses to anti-PD-1 therapy at the level of the tumor microenvironment (12), thus we next examined the relationship between the gut microbiota and systemic and anti-tumor immune responses in our cohort of patients on anti-PD-1 therapy. We compared the tumor-associated immune infiltrates via multi-parameter immunohistochemistry (IHC) and observed a higher density of CD8+ T cells in baseline samples of R versus NR ($p$=0.04), consistent with prior reports (Fig. 4A and fig. S18) (18, 37). Pairwise comparisons using Spearman rank correlations were then performed between specific bacterial taxa enriched in the gut microbiome of R and NR and immune markers in the tumor microenvironment, demonstrating a statistically significant positive correlation between the CD8+ T cell infiltrate in the tumor and abundance of the *Faecalibacterium*

genus, the Ruminococcaceae family and the Clostridiales order in the gut and a non-significant but negative correlation with Bacteroidales (Fig. 4, B and C, and figs. S19 and S20). No associations were seen between CD8+ T cell density and diversity or crOTU community type membership (fig. S21). Analysis of systemic immune responses via flow cytometry and cytokine assays revealed that patients with a high abundance of Clostridiales, Ruminococcaceae or *Faecalibacterium* in the gut had higher levels of effector CD4+ and CD8+ T cells in the systemic circulation with a preserved cytokine response to anti-PD-1 therapy, whereas patients with a higher abundance of Bacteroidales in the gut microbiome had higher levels of regulatory T cells (Treg) and myeloid derived suppressor cells (MDSC) in the systemic circulation, with a blunted cytokine response (Fig. 4D and figs. S22 and S23). To better understand the influence of compositional differences in the gut microbiome on antigen processing and presentation within the tumor microenvironment, we next performed multiplex IHC targeting the myeloid compartment (38). In these studies, patients with a high abundance of *Faecalibacterium* in the gut microbiome had a higher density of immune cells and markers of antigen processing and presentation compared to those with a high abundance of Bacteroidales (Fig. 4, E and F, and figs. S24 and S25), suggesting a possible mechanism through which the gut microbiome may modulate anti-tumor immune responses (12), though this must be validated in a larger cohort.

To investigate a causal link between a “favorable” gut microbiome and response to immune checkpoint blockade, we performed Fecal Microbiome Transplantation (FMT) experiments in germ-free recipient mice (Fig. 4G). In these studies, mice that were transplanted with stool from R to anti-PD-1 therapy (R-FMT) had significantly reduced tumor growth ($p=0.04$, Fig. 4H and fig. S26A) by day 14 compared to those transplanted with stool from NR (NR-FMT). Importantly, mice transplanted with R-FMT also exhibited improved responses to anti-PD-L1 therapy (Fig. 4I) in contrast to mice that were transplanted with stool from NR (NR-FMT). Next we performed 16S sequencing on fecal samples collected from mice treated with FMT, demonstrating that R-FMT mice also had significantly higher abundance of *Faecalibacterium* in their gut microbiome ($p<0.01$) (fig. S27). We also wanted to better understand the mechanism through which the gut microbiome may influence systemic and anti-tumor immune responses, and performed correlative studies on tumors, peripheral blood and spleens from these mice. These studies demonstrated that tumors of mice receiving R-FMT had a higher density of CD8+ T cells than mice receiving NR-FMT, consistent with human data (Fig. 4J and fig. S26B, top series). Analysis of CD45+ myeloid and lymphoid tumor infiltrating cells by flow cytometry confirmed this result (fig. S26C). Moreover, FMT from R locally increased the number of CD45+ immune and CD8+ T cells in the gut compared to NR-FMT (Fig. 4K and fig. S26B, bottom series). Mass cytometry analysis using t-SNE dimension reduction was performed on tumors from mice, and demonstrated up-regulation of PD-L1 in the tumor microenvironment of mice receiving R-FMT versus NR-FMT (fig. S26D), suggesting the development of a “hot” tumor microenvironment. Further phenotypic studies of tumor immune infiltrates revealed a significant enrichment of innate effector cells (expressing CD45+CD11b+Ly6G+) in mice receiving R-FMT (fig. S26E). A lower frequency of suppressive myeloid cells (expressing CD11b+CD11c+) was observed in mice receiving R-FMT compared to mice receiving NR-FMT (fig. S26F). Finally, an increase in the frequency of RORγT+ Th17 cells in the tumor was also detected

in NR-FMT mice (fig. S26G), in line with what we observed in tumors from patients who failed to respond to anti-PD-1 therapy. Mice receiving NR-FMT also had higher levels of regulatory CD4+ FoxP3+ T cells (fig. S26H) and CD4+ IL-17+ (fig. S26I) cells in the spleen, suggesting impaired host immune responses.

Our results indicate that the gut microbiome may modulate responses to anti PD-1 immunotherapy in melanoma patients. We propose that patients with a “favorable” gut microbiome (e.g., high diversity and abundance of Ruminococcaceae/*Faecalibacterium*) have enhanced systemic and anti-tumor immune responses mediated by increased antigen presentation, and improved effector T cell function in the periphery and the tumor microenvironment. In contrast, patients with an “unfavorable” gut microbiome (e.g., low diversity and high relative abundance of Bacteroidales) have impaired systemic and anti-tumor immune responses mediated by limited intratumoral lymphoid and myeloid infiltration and weakened antigen presentation capacity. These findings highlight the therapeutic potential of modulating the gut microbiome in patients receiving checkpoint blockade immunotherapy, and warrant prompt evaluation in cancer patients through clinical trials.

## Supplementary Material

Refer to Web version on PubMed Central for supplementary material.

## Authors

V. Gopalakrishnan[1,2,*], C. N. Spencer[2,3,*], L. Nezi[3,*], A. Reuben[1], M. C. Andrews[1], T. V. Karpinets[3], P. A. Prieto[1,†], D. Vicente[1], K. Hoffman[4], S. C. Wei[5], A. P. Cogdill[1,5], L. Zhao[3], C. W. Hudgens[6], D. S. Hutchinson[7], T. Manzo[3], M. Petaccia de Macedo[6,‡], T. Cotechini[8], T. Kumar[3], W. S. Chen[9], S. M. Reddy[10], R. Szczepaniak Sloane[1], J. Galloway-Pena[11], H. Jiang[1], P. L. Chen[9,§], E. J. Shpall[12], K. Rezvani[12], A. M. Alousi[12], R. F. Chemaly[11], S. Shelburne[3,11], L. M. Vence[5], P. C. Okhuysen[11], V. B. Jensen[13], A. G. Swennes[7], F. McAllister[14], E. Marcelo Riquelme Sanchez[14], Y. Zhang[14], E. Le Chatelier[15], L. Zitvogel[16], N. Pons[15], J. L. Austin-Breneman[1,‖], L. E. Haydu[1], E. M. Burton[1], J. M. Gardner[1], E. Sirmans[17], J. Hu[18], A. J. Lazar[6,9], T. Tsujikawa[8], A. Diab[17], H. Tawbi[17], I. C. Glitza[17], W. J. Hwu[17], S. P. Patel[17], S. E. Woodman[17], R. N. Amaria[17], M. A. Davies[17], J. E. Gershenwald[1], P. Hwu[17], J. E. Lee[1], J. Zhang[3], L. M. Coussens[8], Z. A. Cooper[1,3,¶], P. A. Futreal[3], C. R. Daniel[4,2], N. J. Ajami[7], J. F. Petrosino[7], M. T. Tetzlaff[6,9], P. Sharma[5,19], J. P. Allison[5], R. R. Jenq[3,#], and J. A. Wargo[1,3,#,**]

## Affiliations

[1]Department of Surgical Oncology, The University of Texas MD Anderson Cancer Center, Houston, TX 77030, USA

[2]Department of Epidemiology, Human Genetics and Environmental Sciences, University of Texas School of Public Health, Houston, TX 77030, USA

[3]Department of Genomic Medicine, The University of Texas MD Anderson Cancer Center, Houston, TX 77030, USA

[4]Department of Epidemiology, The University of Texas MD Anderson Cancer Center, Houston, TX 77030, USA

[5]Department of Immunology, The University of Texas MD Anderson Cancer Center, Houston, TX 77030, USA

[6]Department of Translational Molecular Pathology, The University of Texas MD Anderson Cancer Center, Houston, TX 77030, USA

[7]Department of Molecular Virology and Microbiology, Baylor College of Medicine, Houston, TX 77030, USA

[8]Department of Cell, Developmental and Cell Biology, Oregon Health and Sciences University, Portland, OR 97239, USA

[9]Department of Pathology, The University of Texas MD Anderson Cancer Center, Houston, TX 77030, USA

[10]Department of Breast Medical Oncology, The University of Texas MD Anderson Cancer Center, Houston, TX 77030, USA

[11]Department of Infectious Diseases, The University of Texas MD Anderson Cancer Center, Houston, TX 77030, USA

[12]Department of Stem Cell Transplantation, The University of Texas MD Anderson Cancer Center, Houston, TX 77030, USA

[13]Department of Veterinary Medicine and Surgery, The University of Texas MD Anderson Cancer Center, Houston, TX 77030, USA

[14]Department of Clinical Cancer Prevention, The University of Texas MD Anderson Cancer Center, Houston, TX 77030, USA

[15]Centre de Recherche de Jouy-en-Josas, Institut National de la Recherche Agronomique, 78352 Jouy-en-Josas, France

[16]Centre d'Investigation Clinique Biothérapie, Institut Gustave-Roussy, 94805 Villejuif Cedex, France

[17]Department of Melanoma Medical Oncology, The University of Texas MD Anderson Cancer Center, Houston, TX 77030, USA

[18]Department of Biostatistics, The University of Texas MD Anderson Cancer Center, Houston, TX 77030, USA

[19]Department of Genitourinary Medical Oncology, The University of Texas MD Anderson Cancer Center, Houston, TX 77030, USA

## Acknowledgments

The data reported in this paper are tabulated in the main text and Supplementary Materials. The authors wish to acknowledge all patients and families affected by melanoma. J.A.W. is supported by the Binational Science

Foundation, the Melanoma Research Alliance, Stand Up To Cancer, an Institutional Research Grant, a Multidisciplinary Research Program Grant, and MD Anderson's Melanoma Moon Shot Program. This project was supported by the generous philanthropic contributions to The University of Texas MD Anderson Melanoma Moon Shots program. J.A.W, P.S and J.P.A are members of the Parker Institute for Cancer Immunotherapy at M. D. Anderson Cancer Center. A.R. is supported by the Kimberley Clarke Foundation Award for Scientific Achievement provided by the Odyssey Fellowship program at The University of Texas MD Anderson Cancer Center. K.L.H. is supported by the NCI/NIH under Award Numbers CA016672 (PI: Ronald DePinho, M.D.) and R25CA057730 (PI: Shine Chang, Ph.D.). J.E.L. is supported by philanthropic contributions to the University of Texas MD Anderson Cancer Center Moon Shots Program, The University of Texas MD Anderson Cancer Center Various Donors Melanoma and Skin Cancers Priority Program Fund, the Miriam and Jim Mulva Research Fund, the McCarthy Skin Cancer Research Fund and the Marit Peterson Fund for Melanoma Research. The authors acknowledge the Miriam and Sheldon G. Adelson Medical Research Foundation for their support of MD Anderson's Biospecimen Collection team. L.M.C acknowledges a Stand Up To Cancer – Lustgarten Foundation Pancreatic Cancer Convergence Dream Team Translational Research Grant, support from the NIH/NCI, and the Brenden-Colson Center for Pancreatic Health. T.T. acknowledges the Oregon Clinical and Translational Research Institute (OCTRI) from the National Center for Advancing Translational Sciences (NCATS) at the NIH (NIH, #UL1TR000128). J.A.W. acknowledges Christine Diaz for administrative support. Fecal, oral and murine 16S, and fecal WGS data are available from the European Nucelotide Archive under accession numbers PRJEB22894, PRJEB22874, PRJEB22895 and PRJEB22893 respectively. Human WES data are available from the European Genome-phenome Archive under accession number EGAS00001002698. J.A.W and V.G. are inventors on a patent application (PCT/US17/53717) submitted by The University of Texas MD Anderson Cancer Center that covers methods to enhance checkpoint blockade therapy by the microbiome. T.T. and L.M.C are inventors on a patent (WO 2017/087847) held by Oregon Health and Science University that covers the multiplex technology. M.A.D. is an advisory board member for Bristol-Myers Squibb, Novartis, GlaxoSmithKline, Roche/Genentech, Sanofi-Aventis, and Vaccinex and has received funding from GlaxoSmithKline, Roche/Genentech, Merck, AstraZeneca, and Sanofi-Aventis. A.J.L. is a consultant for MedImmune, Bristol-Myers Squibb, Novartis, and Merck, and has received research support from AstraZeneca/MedImmune. Z.A.C. is an employee of MedImmune and owns stock or options in AstraZeneca. J.E.G. is on the advisory board of Merck, and receives royalties from Mercator Therapeutics. S.P.P. has honoraria from Speaker's bureau of Dava Oncology, Merck, and Bristol-Myers Squibb, and is an advisory board member for Amgen and Roche/Genentech. P.H. serves on the advisory board of Lion Biotechnologies and Immatics US. R.N.A. has received research support from Merck, Novartis and Bristol-Myers Squibb. P.S. is a consultant for Bristol-Myers Squibb, Jounce Therapeutics, Helsinn, and GlaxoSmithKline as well as a stockholder from Jounce Therapeutics. J.P.A. is a consultant and stockholder for Jounce Therapeutics, receives royalties from Bristol-Myers Squibb, and has intellectual property with Bristol-Myers Squibb and Merck. J.A.W. has received honoraria from Speakers' bureau of Dava Oncology, Bristol-Myers Squibb, Illumina, and is an advisory board member for GlaxoSmithKline, Novartis, and Roche/Genentech.

## References and Notes

1. Schadendorf D, Hodi FS, Robert C, Weber JS, Margolin K, Hamid O, Patt D, Chen T-T, Berman DM, Wolchok JD. Pooled analysis of long-term survival data from phase II and phase III trials of ipilimumab in unresectable or metastatic melanoma. J. Clin. Oncol. 2015; 33:1889–1894. DOI: 10.1200/JCO.2014.56.2736 [PubMed: 25667295]
2. Robert C, et al. KEYNOTE-006 investigators. Pembrolizumab versus ipilimumab in advanced melanoma. N. Engl. J. Med. 2015; 372:2521–2532. DOI: 10.1056/NEJMoa1503093 [PubMed: 25891173]
3. Robert C, Long GV, Brady B, Dutriaux C, Maio M, Mortier L, Hassel JC, Rutkowski P, McNeil C, Kalinka-Warzocha E, Savage KJ, Hernberg MM, Lebbé C, Charles J, Mihalcioiu C, Chiarion-Sileni V, Mauch C, Cognetti F, Arance A, Schmidt H, Schadendorf D, Gogas H, Lundgren-Eriksson L, Horak C, Sharkey B, Waxman IM, Atkinson V, Ascierto PA. Nivolumab in previously untreated melanoma without *BRAF* mutation. N. Engl. J. Med. 2015; 372:320–330. DOI: 10.1056/NEJMoa1412082 [PubMed: 25399552]
4. Vesely MD, Schreiber RD. Cancer immunoediting: Antigens, mechanisms, and implications to cancer immunotherapy. Ann. N. Y. Acad. Sci. 2013; 1284:1–5. DOI: 10.1111/nyas.12105
5. Topalian SL, Drake CG, Pardoll DM. Immune checkpoint blockade: A common denominator approach to cancer therapy. Cancer Cell. 2015; 27:450–461. DOI: 10.1016/j.ccell.2015.03.001 [PubMed: 25858804]
6. Tran E, Robbins PF, Rosenberg SA. 'Final common pathway' of human cancer immunotherapy: Targeting random somatic mutations. Nat. Immunol. 2017; 18:255–262. DOI: 10.1038/ni.3682 [PubMed: 28198830]

7. Bachireddy P, Burkhardt UE, Rajasagi M, Wu CJ. Haematological malignancies: At the forefront of immunotherapeutic innovation. Nat. Rev. Cancer. 2015; 15:201–215. DOI: 10.1038/nrc3907 [PubMed: 25786696]

8. Garrett WS. Cancer and the microbiota. Science. 2015; 348:80–86. DOI: 10.1126/science.aaa4972 [PubMed: 25838377]

9. Segre JA. Microbial growth dynamics and human disease. Science. 2015; 349:1058–1059. DOI: 10.1126/science.aad0781 [PubMed: 26339017]

10. Drewes JL, Housseau F, Sears CL. Sporadic colorectal cancer: Microbial contributors to disease prevention, development and therapy. Br. J. Cancer. 2016; 115:273–280. DOI: 10.1038/bjc.2016.189 [PubMed: 27380134]

11. Paulos CM, Wrzesinski C, Kaiser A, Hinrichs CS, Chieppa M, Cassard L, Palmer DC, Boni A, Muranski P, Yu Z, Gattinoni L, Antony PA, Rosenberg SA, Restifo NP. Microbial translocation augments the function of adoptively transferred self/tumor-specific CD8+ T cells via TLR4 signaling. J. Clin. Invest. 2007; 117:2197–2204. DOI: 10.1172/JCI32205 [PubMed: 17657310]

12. Sivan A, Corrales L, Hubert N, Williams JB, Aquino-Michaels K, Earley ZM, Benyamin FW, Lei YM, Jabri B, Alegre M-L, Chang EB, Gajewski TF. Commensal Bifidobacterium promotes antitumor immunity and facilitates anti–PD-L1 efficacy. Science. 2015; 350:1084–1089. DOI: 10.1126/science.aac4255 [PubMed: 26541606]

13. Iida N, Dzutsev A, Stewart CA, Smith L, Bouladoux N, Weingarten RA, Molina DA, Salcedo R, Back T, Cramer S, Dai R-M, Kiu H, Cardone M, Naik S, Patri AK, Wang E, Marincola FM, Frank KM, Belkaid Y, Trinchieri G, Goldszmid RS. Commensal bacteria control cancer response to therapy by modulating the tumor microenvironment. Science. 2013; 342:967–970. DOI: 10.1126/science.1240527 [PubMed: 24264989]

14. Viaud S, Saccheri F, Mignot G, Yamazaki T, Daillère R, Hannani D, Enot DP, Pfirschke C, Engblom C, Pittet MJ, Schlitzer A, Ginhoux F, Apetoh L, Chachaty E, Woerther P-L, Eberl G, Bérard M, Ecobichon C, Clermont D, Bizet C, Gaboriau-Routhiau V, Cerf-Bensussan N, Opolon P, Yessaad N, Vivier E, Ryffel B, Elson CO, Doré J, Kroemer G, Lepage P, Boneca IG, Ghiringhelli F, Zitvogel L. The intestinal microbiota modulates the anticancer immune effects of cyclophosphamide. Science. 2013; 342:971–976. DOI: 10.1126/science.1240537 [PubMed: 24264990]

15. Schwartz LH, Litière S, de Vries E, Ford R, Gwyther S, Mandrekar S, Shankar L, Bogaerts J, Chen A, Dancey J, Hayes W, Hodi FS, Hoekstra OS, Huang EP, Lin N, Liu Y, Therasse P, Wolchok JD, Seymour L. RECIST 1.1–Update and clarification: From the RECIST committee. Eur. J. Cancer. 2016; 62:132–137. DOI: 10.1016/j.ejca.2016.03.081 [PubMed: 27189322]

16. Snyder A, Makarov V, Merghoub T, Yuan J, Zaretsky JM, Desrichard A, Walsh LA, Postow MA, Wong P, Ho TS, Hollmann TJ, Bruggeman C, Kannan K, Li Y, Elipenahli C, Liu C, Harbison CT, Wang L, Ribas A, Wolchok JD, Chan TA. Genetic basis for clinical response to CTLA-4 blockade in melanoma. N. Engl. J. Med. 2014; 371:2189–2199. DOI: 10.1056/NEJMoa1406498 [PubMed: 25409260]

17. Sharma P, Retz M, Siefker-Radtke A, Baron A, Necchi A, Bedke J, Plimack ER, Vaena D, Grimm M-O, Bracarda S, Arranz JÁ, Pal S, Ohyama C, Saci A, Qu X, Lambert A, Krishnan S, Azrilevich A, Galsky MD. Nivolumab in metastatic urothelial carcinoma after platinum therapy (CheckMate 275): A multicentre, single-arm, phase 2 trial. Lancet Oncol. 2017; 18:312–322. DOI: 10.1016/S1470-2045(17)30065-7 [PubMed: 28131785]

18. Chen PL, Roh W, Reuben A, Cooper ZA, Spencer CN, Prieto PA, Miller JP, Bassett RL, Gopalakrishnan V, Wani K, De Macedo MP, Austin-Breneman JL, Jiang H, Chang Q, Reddy SM, Chen W-S, Tetzlaff MT, Broaddus RJ, Davies MA, Gershenwald JE, Haydu L, Lazar AJ, Patel SP, Hwu P, Hwu W-J, Diab A, Glitza IC, Woodman SE, Vence LM, Wistuba II, Amaria RN, Kwong LN, Prieto V, Davis RE, Ma W, Overwijk WW, Sharpe AH, Hu J, Futreal PA, Blando J, Sharma P, Allison JP, Chin L, Wargo JA. Analysis of immune signatures in longitudinal tumor samples yields insight into biomarkers of response and mechanisms of resistance to immune checkpoint blockade. Cancer Discov. 2016; 6:827–837. DOI: 10.1158/2159-8290.CD-15-1545 [PubMed: 27301722]

19. Roh W, Chen P-L, Reuben A, Spencer CN, Prieto PA, Miller JP, Gopalakrishnan V, Wang F, Cooper ZA, Reddy SM, Gumbs C, Little L, Chang Q, Chen W-S, Wani K, De Macedo MP, Chen E, Austin-Breneman JL, Jiang H, Roszik J, Tetzlaff MT, Davies MA, Gershenwald JE, Tawbi H,

Lazar AJ, Hwu P, Hwu W-J, Diab A, Glitza IC, Patel SP, Woodman SE, Amaria RN, Prieto VG, Hu J, Sharma P, Allison JP, Chin L, Zhang J, Wargo JA, Futreal PA. Integrated molecular analysis of tumor biopsies on sequential CTLA-4 and PD-1 blockade reveals markers of response and resistance. Sci. Transl. Med. 2017; 9 eaah3560. doi: 10.1126/scitranslmed.aah3560

20. Van Allen EM, Miao D, Schilling B, Shukla SA, Blank C, Zimmer L, Sucker A, Hillen U, Foppen MHG, Goldinger SM, Utikal J, Hassel JC, Weide B, Kaehler KC, Loquai C, Mohr P, Gutzmer R, Dummer R, Gabriel S, Wu CJ, Schadendorf D, Garraway LA. Genomic correlates of response to CTLA-4 blockade in metastatic melanoma. Science. 2015; 350:207–211. DOI: 10.1126/science.aad0095 [PubMed: 26359337]
21. McGranahan N, Furness AJS, Rosenthal R, Ramskov S, Lyngaa R, Saini SK, Jamal-Hanjani M, Wilson GA, Birkbak NJ, Hiley CT, Watkins TBK, Shafi S, Murugaesu N, Mitter R, Akarca AU, Linares J, Marafioti T, Henry JY, Van Allen EM, Miao D, Schilling B, Schadendorf D, Garraway LA, Makarov V, Rizvi NA, Snyder A, Hellmann MD, Merghoub T, Wolchok JD, Shukla SA, Wu CJ, Peggs KS, Chan TA, Hadrup SR, Quezada SA, Swanton C. Clonal neoantigens elicit T cell immunoreactivity and sensitivity to immune checkpoint blockade. Science. 2016; 351:1463–1469. DOI: 10.1126/science.aaf1490 [PubMed: 26940869]
22. Hugo W, Zaretsky JM, Sun L, Song C, Moreno BH, Hu-Lieskovan S, Berent-Maoz B, Pang J, Chmielowski B, Cherry G, Seja E, Lomeli S, Kong X, Kelley MC, Sosman JA, Johnson DB, Ribas A, Lo RS. Genomic and transcriptomic features of response to anti-PD-1 therapy in metastatic melanoma. Cell. 2016; 165:35–44. DOI: 10.1016/j.cell.2016.02.065 [PubMed: 26997480]
23. Johnson DB, Frampton GM, Rioth MJ, Yusko E, Xu Y, Guo X, Ennis RC, Fabrizio D, Chalmers ZR, Greenbowe J, Ali SM, Balasubramanian S, Sun JX, He Y, Frederick DT, Puzanov I, Balko JM, Cates JM, Ross JS, Sanders C, Robins H, Shyr Y, Miller VA, Stephens PJ, Sullivan RJ, Sosman JA, Lovly CM. Targeted next generation sequencing identifies markers of response to PD-1 blockade. Cancer Immunol. Res. 2016; 4:959–967. DOI: 10.1158/2326-6066.CIR-16-0143 [PubMed: 27671167]
24. Rizvi NA, Hellmann MD, Snyder A, Kvistborg P, Makarov V, Havel JJ, Lee W, Yuan J, Wong P, Ho TS, Miller ML, Rekhtman N, Moreira AL, Ibrahim F, Bruggeman C, Gasmi B, Zappasodi R, Maeda Y, Sander C, Garon EB, Merghoub T, Wolchok JD, Schumacher TN, Chan TA. Mutational landscape determines sensitivity to PD-1 blockade in non-small cell lung cancer. Science. 2015; 348:124–128. DOI: 10.1126/science.aaa1348 [PubMed: 25765070]
25. Muegge BD, Kuczynski J, Knights D, Clemente JC, González A, Fontana L, Henrissat B, Knight R, Gordon JI. Diet drives convergence in gut microbiome functions across mammalian phylogeny and within humans. Science. 2011; 332:970–974. DOI: 10.1126/science.1198719 [PubMed: 21596990]
26. Human Microbiome Project Consortium. Structure, function and diversity of the healthy human microbiome. Nature. 2012; 486:207–214. DOI: 10.1038/nature11234 [PubMed: 22699609]
27. Turnbaugh PJ, Bäckhed F, Fulton L, Gordon JI. Diet-induced obesity is linked to marked but reversible alterations in the mouse distal gut microbiome. Cell Host Microbe. 2008; 3:213–223. DOI: 10.1016/j.chom.2008.02.015 [PubMed: 18407065]
28. Qin J, et al. MetaHIT Consortium. A human gut microbial gene catalogue established by metagenomic sequencing. Nature. 2010; 464:59–65. DOI: 10.1038/nature08821 [PubMed: 20203603]
29. Taur Y, Jenq RR, Perales M-A, Littmann ER, Morjaria S, Ling L, No D, Gobourne A, Viale A, Dahi PB, Ponce DM, Barker JN, Giralt S, van den Brink M, Pamer EG. The effects of intestinal tract bacterial diversity on mortality following allogeneic hematopoietic stem cell transplantation. Blood. 2014; 124:1174–1182. DOI: 10.1182/blood-2014-02-554725 [PubMed: 24939656]
30. Lozupone C, Lladser ME, Knights D, Stombaugh J, Knight R. UniFrac: An effective distance metric for microbial community comparison. ISME J. 2011; 5:169–172. DOI: 10.1038/ismej.2010.133 [PubMed: 20827291]
31. Segata N, Izard J, Waldron L, Gevers D, Miropolsky L, Garrett WS, Huttenhower C. Metagenomic biomarker discovery and explanation. Genome Biol. 2011; 12:R60.doi: 10.1186/gb-2011-12-6-r60 [PubMed: 21702898]
32. Peled JU, Devlin SM, Staffas A, Lumish M, Khanin R, Littmann ER, Ling L, Kosuri S, Maloy M, Slingerland JB, Ahr KF, Porosnicu Rodriguez KA, Shono Y, Slingerland AE, Docampo MD, Sung

AD, Weber D, Alousi AM, Gyurkocza B, Ponce DM, Barker JN, Perales M-A, Giralt SA, Taur Y, Pamer EG, Jenq RR, van den Brink MRM. Intestinal microbiota and relapse after hematopoietic-cell transplantation. J. Clin. Oncol. 2017; 35:1650–1659. DOI: 10.1200/JCO.2016.70.3348 [PubMed: 28296584]

33. Chaput N, Lepage P, Coutzac C, Soularue E, Le Roux K, Monot C, Boselli L, Routier E, Cassard L, Collins M, Vaysse T, Marthey L, Eggermont A, Asvatourian V, Lanoy E, Mateus C, Robert C, Carbonnel F. Baseline gut microbiota predicts clinical response and colitis in metastatic melanoma patients treated with ipilimumab. Ann. Oncol. 2017; 28:1368–1379. DOI: 10.1093/annonc/mdx108 [PubMed: 28368458]
34. Caspi R, Foerster H, Fulcher CA, Kaipa P, Krummenacker M, Latendresse M, Paley S, Rhee SY, Shearer AG, Tissier C, Walk TC, Zhang P, Karp PD. The MetaCyc Database of metabolic pathways and enzymes and the BioCyc collection of Pathway/Genome Databases. Nucleic Acids Res. 2008; 36:D623–D631. DOI: 10.1093/nar/gkm900 [PubMed: 17965431]
35. Kanehisa M, Goto S. KEGG: Kyoto encyclopedia of genes and genomes. Nucleic Acids Res. 2000; 28:27–30. DOI: 10.1093/nar/28.1.27 [PubMed: 10592173]
36. Blacher E, Levy M, Tatirovsky E, Elinav E. Microbiome-modulated metabolites at the interface of host immunity. J. Immunol. 2017; 198:572–580. DOI: 10.4049/jimmunol.1601247 [PubMed: 28069752]
37. Tumeh PC, Harview CL, Yearley JH, Shintaku IP, Taylor EJM, Robert L, Chmielowski B, Spasic M, Henry G, Ciobanu V, West AN, Carmona M, Kivork C, Seja E, Cherry G, Gutierrez AJ, Grogan TR, Mateus C, Tomasic G, Glaspy JA, Emerson RO, Robins H, Pierce RH, Elashoff DA, Robert C, Ribas A. PD-1 blockade induces responses by inhibiting adaptive immune resistance. Nature. 2014; 515:568–571. DOI: 10.1038/nature13954 [PubMed: 25428505]
38. Tsujikawa T, Kumar S, Borkar RN, Azimi V, Thibault G, Chang YH, Balter A, Kawashima R, Choe G, Sauer D, El Rassi E, Clayburgh DR, Kulesz-Martin MF, Lutz ER, Zheng L, Jaffee EM, Leyshock P, Margolin AA, Mori M, Gray JW, Flint PW, Coussens LM. Quantitative multiplex immunohistochemistry reveals myeloid-inflamed tumor-immune complexity associated with poor prognosis. Cell Reports. 2017; 19:203–217. DOI: 10.1016/j.celrep.2017.03.037 [PubMed: 28380359]
39. Human Microbiome Project Consortium. A framework for human microbiome research. Nature. 2012; 486:215–221. DOI: 10.1038/nature11209 [PubMed: 22699610]
40. Caporaso JG, Lauber CL, Walters WA, Berg-Lyons D, Huntley J, Fierer N, Owens SM, Betley J, Fraser L, Bauer M, Gormley N, Gilbert JA, Smith G, Knight R. Ultra-high-throughput microbial community analysis on the Illumina HiSeq and MiSeq platforms. ISME J. 2012; 6:1621–1624. DOI: 10.1038/ismej.2012.8 [PubMed: 22402401]
41. Rognes T, Flouri T, Nichols B, Quince C, Mahé F. VSEARCH: A versatile open source tool for metagenomics. PeerJ. 2016; 4:e2584.doi: 10.7717/peerj.2584 [PubMed: 27781170]
42. Edgar RC. Search and clustering orders of magnitude faster than BLAST. Bioinformatics. 2010; 26:2460–2461. DOI: 10.1093/bioinformatics/btq461 [PubMed: 20709691]
43. Edgar RC. UPARSE: Highly accurate OTU sequences from microbial amplicon reads. Nat. Methods. 2013; 10:996–998. DOI: 10.1038/nmeth.2604 [PubMed: 23955772]
44. DeSantis TZ, Hugenholtz P, Larsen N, Rojas M, Brodie EL, Keller K, Huber T, Dalevi D, Hu P, Andersen GL. Greengenes, a chimera-checked 16S rRNA gene database and workbench compatible with ARB. Appl. Environ. Microbiol. 2006; 72:5069–5072. DOI: 10.1128/AEM.03006-05 [PubMed: 16820507]
45. Cole JR, Wang Q, Fish JA, Chai B, McGarrell DM, Sun Y, Brown CT, Porras-Alfaro A, Kuske CR, Tiedje JM. Ribosomal Database Project: Data and tools for high throughput rRNA analysis. Nucleic Acids Res. 2014; 42:D633–D642. DOI: 10.1093/nar/gkt1244 [PubMed: 24288368]
46. Quast C, Pruesse E, Yilmaz P, Gerken J, Schweer T, Yarza P, Peplies J, Glöckner FO. The SILVA ribosomal RNA gene database project: Improved data processing and web-based tools. Nucleic Acids Res. 2013; 41:D590–D596. DOI: 10.1093/nar/gks1219 [PubMed: 23193283]
47. Caporaso JG, Bittinger K, Bushman FD, DeSantis TZ, Andersen GL, Knight R. PyNAST: A flexible tool for aligning sequences to a template alignment. Bioinformatics. 2010; 26:266–267. DOI: 10.1093/bioinformatics/btp636 [PubMed: 19914921]

48. Schloss PD, Westcott SL, Ryabin T, Hall JR, Hartmann M, Hollister EB, Lesniewski RA, Oakley BB, Parks DH, Robinson CJ, Sahl JW, Stres B, Thallinger GG, Van Horn DJ, Weber CF. Introducing mothur: Open-source, platform-independent, community-supported software for describing and comparing microbial communities. Appl. Environ. Microbiol. 2009; 75:7537–7541. DOI: 10.1128/AEM.01541-09 [PubMed: 19801464]
49. Price MN, Dehal PS, Arkin AP. FastTree 2—approximately maximum-likelihood trees for large alignments. PLOS ONE. 2010; 5:e9490.doi: 10.1371/journal.pone.0009490 [PubMed: 20224823]
50. Caporaso JG, Kuczynski J, Stombaugh J, Bittinger K, Bushman FD, Costello EK, Fierer N, Peña AG, Goodrich JK, Gordon JI, Huttley GA, Kelley ST, Knights D, Koenig JE, Ley RE, Lozupone CA, McDonald D, Muegge BD, Pirrung M, Reeder J, Sevinsky JR, Turnbaugh PJ, Walters WA, Widmann J, Yatsunenko T, Zaneveld J, Knight R. QIIME allows analysis of high-throughput community sequencing data. Nat. Methods. 2010; 7:335–336. DOI: 10.1038/nmeth.f.303 [PubMed: 20383131]
51. Yutin N, Galperin MY. A genomic update on clostridial phylogeny: Gram-negative spore formers and other misplaced clostridia. Environ. Microbiol. 2013; 15:2631–2641. [PubMed: 23834245]
52. Lozupone C, Knight R. UniFrac: A new phylogenetic method for comparing microbial communities. Appl. Environ. Microbiol. 2005; 71:8228–8235. DOI: 10.1128/AEM.71.12.8228-8235.2005 [PubMed: 16332807]
53. Morgan XC, Huttenhower C. Chapter 12: Human microbiome analysis. PLOS Comput. Biol. 2012; 8:e1002808.doi: 10.1371/journal.pcbi.1002808 [PubMed: 23300406]
54. Chao A. Nonparametric estimation of the number of classes in a population. Scand. J. Stat. 1984; 11:265–270.
55. Simpson EH. Measurement of diversity. Nature. 1949; 163:688–688. DOI: 10.1038/163688a0
56. Shannon CE. A mathematical theory of communication. Mob. Comput. Commun. Rev. 2001; 5:3–55. DOI: 10.1145/584091.584093
57. Shannon CE, Weaver W. A mathematical theory of communication. Bell Syst. Tech. J. 1948; 27:623–656. DOI: 10.1002/j.1538-7305.1948.tb00917.x
58. Shannon PT, Grimes M, Kutlu B, Bot JJ, Galas DJ. RCytoscape: Tools for exploratory network analysis. BMC Bioinformatics. 2013; 14:217.doi: 10.1186/1471-2105-14-217 [PubMed: 23837656]
59. Li J, et al. MetaHIT Consortium. An integrated catalog of reference genes in the human gut microbiome. Nat. Biotechnol. 2014; 32:834–841. DOI: 10.1038/nbt.2942 [PubMed: 24997786]
60. Langmead B, Salzberg SL. Fast gapped-read alignment with Bowtie 2. Nat. Methods. 2012; 9:357–359. DOI: 10.1038/nmeth.1923 [PubMed: 22388286]
61. Cotillard A, et al. ANR MicroObes Consortium. Dietary intervention impact on gut microbial gene richness. Nature. 2013; 500:585–588. DOI: 10.1038/nature12480 [PubMed: 23985875]
62. Pons, N., Batto, J-M., Kennedy, S., Almeida, M., Boumezbeur, F. paper presented at the Annual Conference of the JOBIM (Journées Ouvertes en Biologie, Informatique et Mathématique); Montpellier, France. 7 to 9 September 2010;
63. Nielsen HB, et al. MetaHIT Consortium. Identification and assembly of genomes and genetic elements in complex metagenomic samples without using reference genomes. Nat. Biotechnol. 2014; 32:822–828. DOI: 10.1038/nbt.2939 [PubMed: 24997787]
64. Li H, Durbin R. Fast and accurate short read alignment with Burrows-Wheeler transform. Bioinformatics. 2009; 25:1754–1760. DOI: 10.1093/bioinformatics/btp324 [PubMed: 19451168]
65. McKenna A, Hanna M, Banks E, Sivachenko A, Cibulskis K, Kernytsky A, Garimella K, Altshuler D, Gabriel S, Daly M, DePristo MA. The Genome Analysis Toolkit: A MapReduce framework for analyzing next-generation DNA sequencing data. Genome Res. 2010; 20:1297–1303. DOI: 10.1101/gr.107524.110 [PubMed: 20644199]
66. Cibulskis K, Lawrence MS, Carter SL, Sivachenko A, Jaffe D, Sougnez C, Gabriel S, Meyerson M, Lander ES, Getz G. Sensitive detection of somatic point mutations in impure and heterogeneous cancer samples. Nat. Biotechnol. 2013; 31:213–219. DOI: 10.1038/nbt.2514 [PubMed: 23396013]
67. Ye K, Schulz MH, Long Q, Apweiler R, Ning Z. Pindel: A pattern growth approach to detect break points of large deletions and medium sized insertions from paired-end short reads. Bioinformatics. 2009; 25:2865–2871. DOI: 10.1093/bioinformatics/btp394 [PubMed: 19561018]

68. Sachidanandam R, et al. International SNP Map Working Group. A map of human genome sequence variation containing 1.42 million single nucleotide polymorphisms. Nature. 2001; 409:928–933. DOI: 10.1038/35057149 [PubMed: 11237013]
69. 1000 Genomes Project Consortium. An integrated map of genetic variation from 1,092 human genomes. Nature. 2012; 491:56–65. DOI: 10.1038/nature11632 [PubMed: 23128226]
70. Lek M, et al. Exome Aggregation Consortium. Analysis of protein-coding genetic variation in 60,706 humans. Nature. 2016; 536:285–291. DOI: 10.1038/nature19057 [PubMed: 27535533]
71. Fu W, O'Connor TD, Jun G, Kang HM, Abecasis G, Leal SM, Gabriel S, Rieder MJ, Altshuler D, Shendure J, Nickerson DA, Bamshad MJ, Akey JM. NHLBI Exome Sequencing Project. Analysis of 6,515 exomes reveals the recent origin of most human protein-coding variants. Nature. 2013; 493:216–220. DOI: 10.1038/nature11690 [PubMed: 23201682]
72. Zhang T, Dutton-Regester K, Brown KM, Hayward NK. The genomic landscape of cutaneous melanoma. Pigment Cell Melanoma Res. 2016; 29:266–283. DOI: 10.1111/pcmr.12459 [PubMed: 26833684]
73. Cooper ZA, Reuben A, Spencer CN, Prieto PA, Austin-Breneman JL, Jiang H, Haymaker C, Gopalakrishnan V, Tetzlaff MT, Frederick DT, Sullivan RJ, Amaria RN, Patel SP, Hwu P, Woodman SE, Glitza IC, Diab A, Vence LM, Rodriguez-Canales J, Parra ER, Wistuba II, Coussens LM, Sharpe AH, Flaherty KT, Gershenwald JE, Chin L, Davies MA, Clise-Dwyer K, Allison JP, Sharma P, Wargo JA. Distinct clinical patterns and immune infiltrates are observed at time of progression on targeted therapy versus immune checkpoint blockade for melanoma. Oncoimmunology. 2016; 5:e1136044. [PubMed: 27141370]
74. Blanche P, Dartigues JF, Jacqmin-Gadda H. Estimating and comparing time-dependent areas under receiver operating characteristic curves for censored event times with competing risks. Stat. Med. 2013; 32:5381–5397. DOI: 10.1002/sim.5958 [PubMed: 24027076]
75. Fritz CO, Morris PE, Richler JJ. Effect size estimates: Current use, calculations, and interpretation. J. Exp. Psychol. Gen. 2012; 141:2–18. DOI: 10.1037/a0024338 [PubMed: 21823805]
76. R Development Core Team. R Foundation for Statistical Computing. Vienna, Austria: 2017.
77. National Research Council. Guide for the Care and Use of Laboratory Animals. 8. National Academies Press; 2011. p. 1-220.
78. Cooper ZA, Juneja VR, Sage PT, Frederick DT, Piris A, Mitra D, Lo JA, Hodi FS, Freeman GJ, Bosenberg MW, McMahon M, Flaherty KT, Fisher DE, Sharpe AH, Wargo JA. Response to BRAF inhibition in melanoma is enhanced when combined with immune checkpoint blockade. Cancer Immunol. Res. 2014; 2:643–654. DOI: 10.1158/2326-6066.CIR-13-0215 [PubMed: 24903021]
79. Amir ED, Davis KL, Tadmor MD, Simonds EF, Levine JH, Bendall SC, Shenfeld DK, Krishnaswamy S, Nolan GP, Pe'er D. viSNE enables visualization of high dimensional single-cell data and reveals phenotypic heterogeneity of leukemia. Nat. Biotechnol. 2013; 31:545–552. DOI: 10.1038/nbt.2594 [PubMed: 23685480]

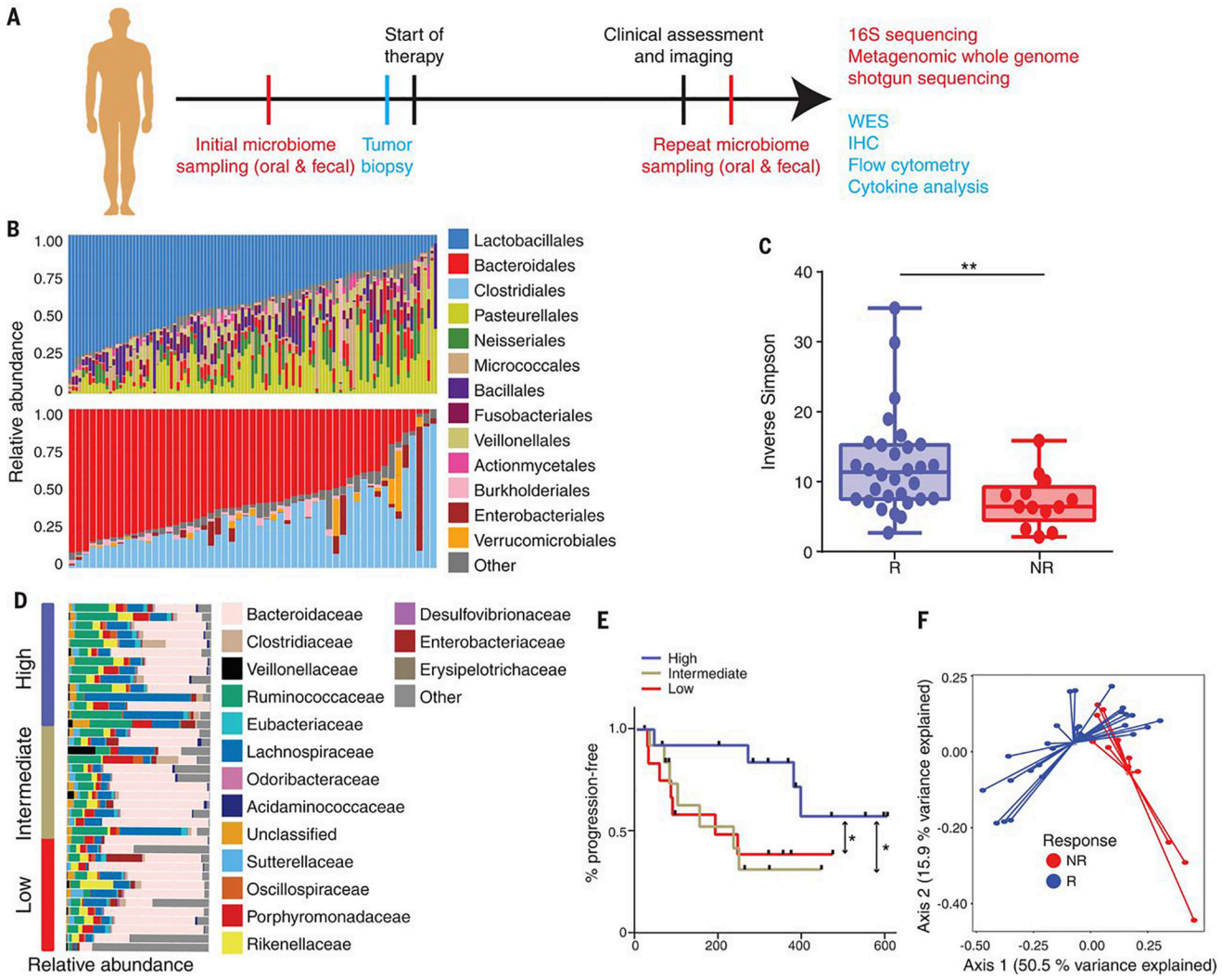


**Figure 1. Enhanced gut microbiome diversity is associated with improved response to anti-PD-1 immunotherapy in patients with metastatic melanoma**

(**A**) Schema of sample collection and analyses. (**B**) Stacked bar plot of phylogenetic composition of common bacterial taxa (>0.1% abundance) at the order level in oral (n=109, top) and fecal (n=53, bottom) samples by 16S rRNA sequencing. (**C**) Inverse Simpson diversity scores of the gut microbiome in R (n=30) and NR (n=13) to anti PD-1 immunotherapy by Mann-Whitney (MW) test. Error bars represent the distribution of diversity scores. (**D**) Phylogenetic composition of fecal samples (n=39) at the family level (>0.1% abundance) at baseline. High (blue) (>11.63, n=13), intermediate (gold) (7.46-11.63, n=13) and low (red) (<7.46, n=13) diversity groups were determined using tertiles of Inverse Simpson scores. (**E**) Kaplan-Meier (KM) plot of progression-free survival (PFS) by fecal diversity; high (median PFS undefined), intermediate (median PFS=232 days), and low (median PFS=188 days). High vs intermediate diversity (HR 3.60, 95% C.I. 1.02-12.74) and high vs low (HR 3.57, 95% C.I. 1.02-12.52) by univariate Cox model. *$p$<0.05, **$p$<0.01. (**F**) Principal coordinate analysis of fecal samples (n=43) by response using Weighted UniFrac distances.

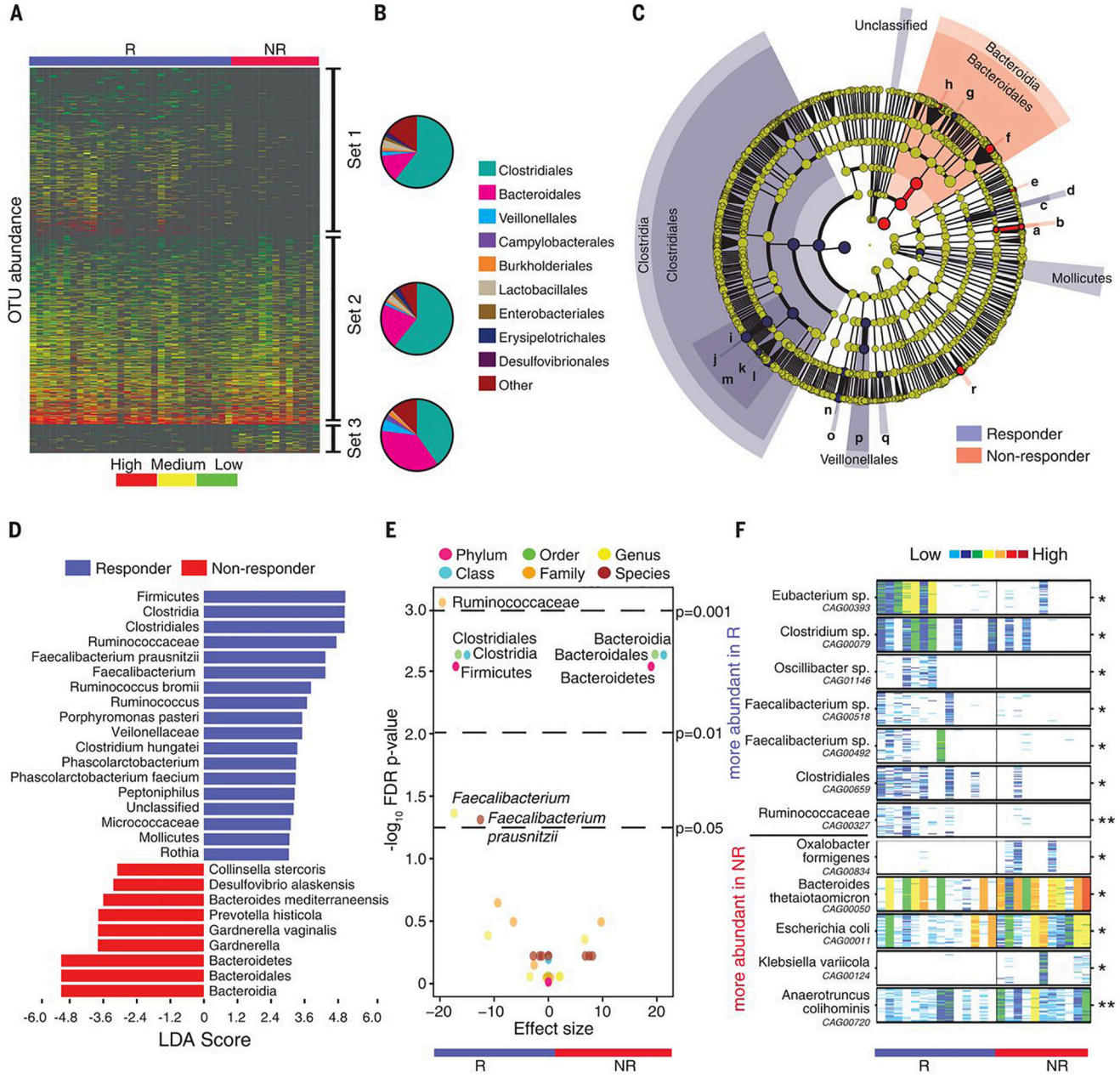


**Figure 2. Compositional differences in the gut microbiome are associated with responses to anti-PD-1 immunotherapy**

(**A**) Heatmap of OTU abundances in R (n=30) and NR (n=13). Columns denote patients grouped by response and sorted by diversity within R and NR groups; rows denote bacterial OTUs grouped into 3 sets according to their enrichment/depletion in R versus NR: Set 1 (enriched in R), Set 2 (unenriched), and Set 3 (enriched in NR), and then sorted by mean abundance within each set. (**B**) Phylogenetic composition of OTUs within each set at the order level. Set 1 (enriched in R); Set 2 (unenriched); Set 3 (enriched in NR). (**C**) Taxonomic cladogram from LEfSe showing differences in fecal taxa. Dot size is proportional to the abundance of the taxon. Letters correspond to the following taxa: (a) *Gardnerella vaginalis*, (b) Gardnerella, (c) *Rothia*, (d) *Micrococcaceae*, (e) *Collinsella*

*stercoris*, (f) *Bacteroides mediterraneensis*, (g) *Porphyromonas pasteri*, (h) *Prevotella histicola*, (i) *Faecalibacterium prausnitzii*, (j) *Faecalibacterium*, (k) *Clostridium hungatei*, (l) *Ruminococcus bromii*, (m) Ruminococcaceae, (n) *Phascolarctobacterium faecium*, (o) *Phascolarctobacterium*, (p) *Veilonellaceae*, (q) *Peptoniphilus*, (r) *Desulfovbrio alaskensis.* (**D**) LDA scores computed for differentially-abundant taxa in the fecal microbiomes of R (blue) and NR (red). Length indicates effect size associated with a taxon. $p$=0.05 for the Kruskal-Wallis test; LDA score > 3. (**E**) Differentially-abundant gut bacteria in R (blue) vs NR (red) by MW test (FDR-adjusted) within all taxonomic levels. (**F**) Pairwise comparisons by MW test of abundances of metagenomic species (MGS) identified by metagenomic WGS in fecal samples (n=25): R (n=14, blue), NR (n=11, red). *$p$<0.05, **$p$<0.01. Colors reflect gene abundances visualized using “barcodes” with the following order of intensity: white(0)<light blue<blue<green<yellow<orange<red for increasing abundance and each color change corresponds to a 4x fold abundance change. In these barcodes, MGS appear as vertical lines (co-abundant genes in a sample) colored according to the gene abundance.

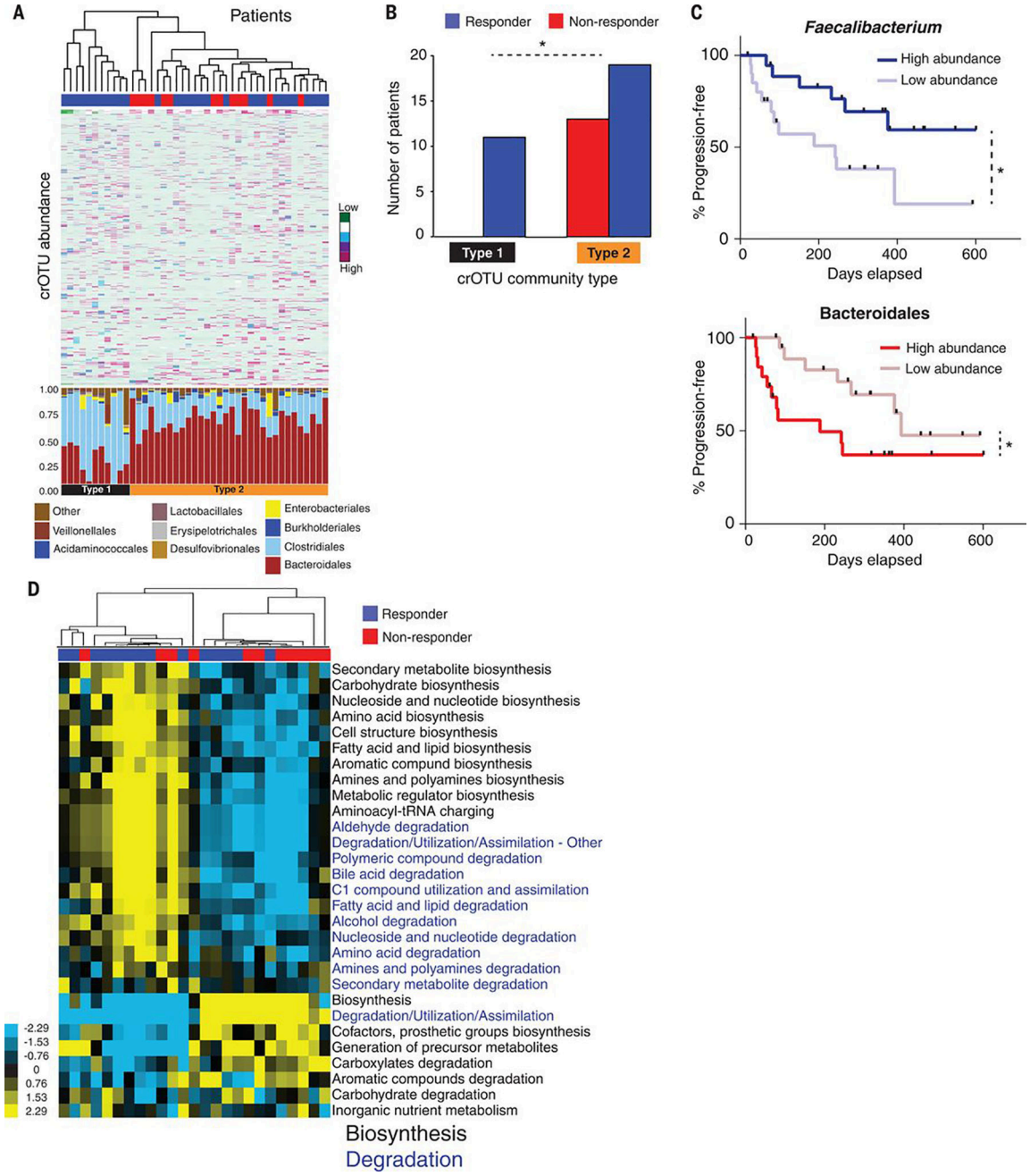


**Figure 3. Abundance of crOTUs within the gut microbiome is predictive of response to anti-PD-1 immunotherapy**

(**A**) Top: Unsupervised hierarchical clustering by complete linkage of Euclidean distances of crOTU abundances in 43 fecal samples. Bottom: Stacked bar plot of relative abundances at the order level by crOTU community-type. (**B**) Association of crOTU community types with response to anti-PD-1 by Fisher's exact test. crOTU community type 1 (black, n=11: R=11, NR=0); crOTU community type 2 (orange, n=32: R=19, NR=13). Blue bars indicate responders, whereas red bars indicate non-responders. (**C**) Comparison KM PFS curves by long-rank test in patients with high abundance (dark blue, n=19, median PFS=undefined) or

low abundance (light blue, n=20, median PFS=242 days) of *Faecalibacterium* (top PFS curve). High abundance (dark red, n=20, median PFS=188 days) or low abundance (light red, n=19, median PFS=393 days) of Bacteroidales (bottom PFS curve). (**D**) Unsupervised hierarchical clustering of pathway class enrichment calculated as the number of MetaCyc pathways predicted in the metagenomes of fecal samples from 25 patients (R=14, NR=11). Columns represent patient samples (blue=R, red=NR) and rows represent enrichment of predicted MetaCyc pathways (blue=low enrichment, black=medium enrichment, yellow= high enrichment). Black text: biosynthetic pathways, blue text: degradative pathways. *$p<0.05$.

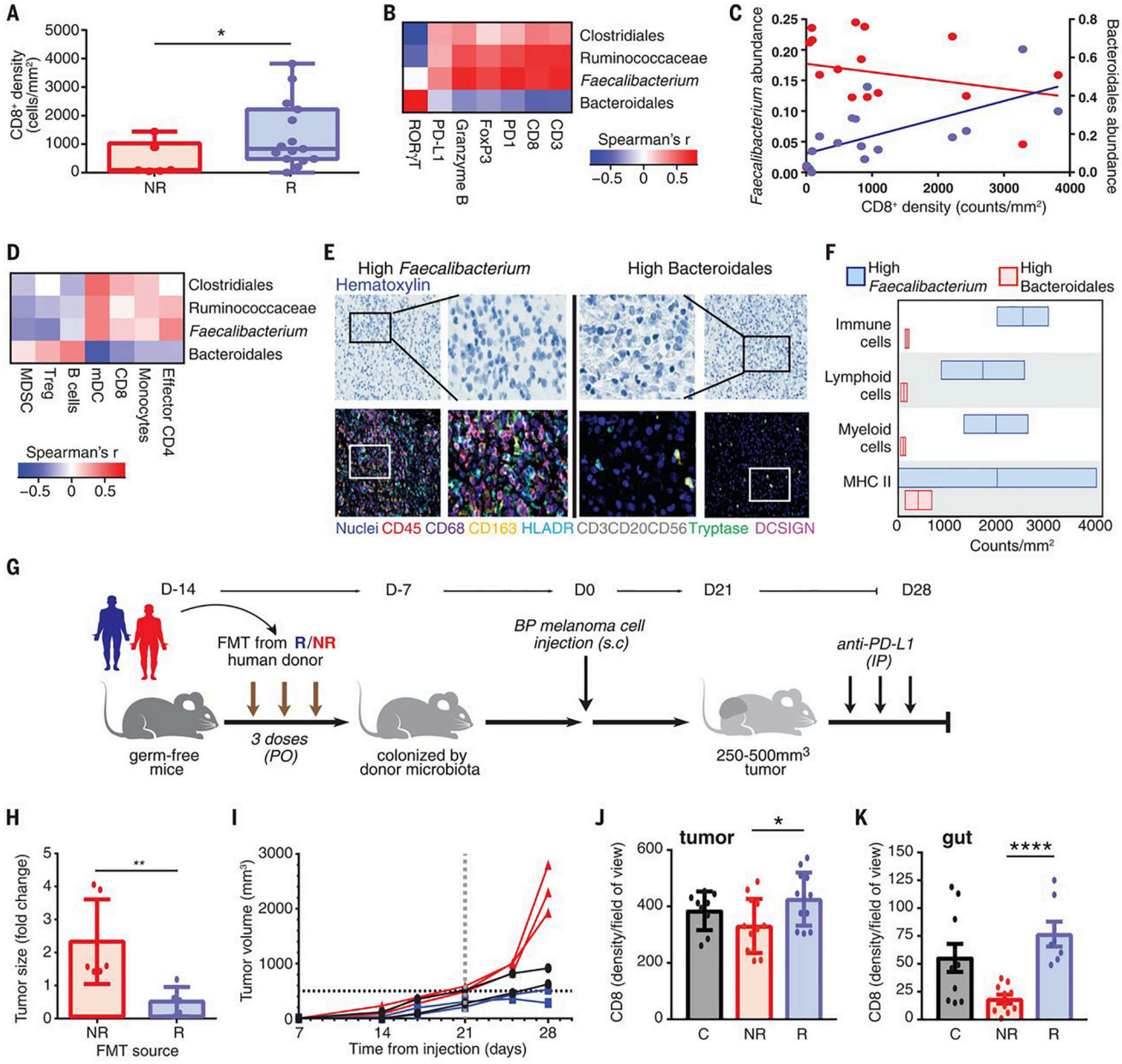


**Figure 4. A favorable gut microbiome is associated with enhanced systemic and anti-tumor immunity**

(**A**) Quantification by IHC of the CD8+ T cell infiltrate at pre-treatment in tumors in R (n=15, blue) and NR (n=6, red) by one-sided MW test. Error bars represent the distribution of CD8+ T cell densities. (**B**) Pairwise Spearman rank correlation heatmap of significantly different taxa in fecal samples (n=15) at baseline and CD3, CD8, PD-1, FoxP3, Granzyme B, PD-L1 and RORγT density by H-score in matched tumors. (**C**) Univariate linear regression between CD8+ counts/mm2 in the tumor versus *Faecalibacterium* (blue, $r^2$=0.42, p<0.01) and Bacteroidales (red, $r^2$=0.06, p=0.38) abundance in the gut. (**D**) Pairwise Spearman rank correlation heatmap between significantly different fecal taxa and frequency of indicated cell types by flow cytometry in peripheral blood at baseline. (**E**) Representative

multiplex IHC images and (**F**) Frequency of various immune cell types in patients having high *Faecalibacterium* (n=2) or Bacteroidales (n=2) in the gut. (**G**) Experimental design of studies in germ-free (GF) mice. Time in days (indicated as D) relative to tumor injection (2.5-8x$10^5$ tumor cells). (**H**) Difference in size by MW test of tumors at day 14, implanted in R-FMT (blue) and NR-FMT mice (red) expressed as fold change (FC) relative to average tumor volume of Control GF mice. Data from 2 independent FMT experiments (R-FMT, n=5, median FC=0.18; NR-FMT, n=6, median FC=1.52). (**I**) Representative tumor growth curves for each GF mouse from α-PD-L1 treated R-FMT (blue n=2, median tumor volume=403.7 $mm^3$), NR-FMT (red n=3, median tumor volume=2301 $mm^3$), and Control (black, n=2, median tumor volume=771.35 $mm^3$) mice. Statistics are as follows: p=0.20 (R-FMT vs NR-FMT), p=0.33 (NR-FMT vs Control) by MW test. Dotted black line marks tumor size cutoff for α-PD-L1 treatment (500$mm^3$). (**J**) Quantification of CD8+ density in tumor of R-FMT (n=2, median=433.5 cells/HPF across 12 regions), NR-FMT (NR-FMT n=2, median=325 cells/HPF across 12 regions) and Control mice (n=2, median=412 cells/HPF across 9 regions). MW test p=0.30 (R-FMT vs Control). (**K**) Quantification of CD8+ density in gut (R-FMT n=2, median=67 cells/HPF across 7 regions), NR-FMT (n=2, median=24 cells/HPF across in 5 regions), Control n=2 (median=47 cells/HPF across 10 regions). MW test p=0.17 (R-FMT vs Control). *$p$<0.05, **$p$<0.01, ****$p$<0.0001.